Available online at www.sciencedirect.com
SCIENCE DIRECT®
PHYSICS LETTERS B
ELSEVIER
Physics Letters B 563 (2003) 35–47
www.elsevier.com/locate/npe

Study of neutrino electromagnetic properties with the prototype of the Borexino detector

H.O. Back [a], M. Balata [b], A. de Bari [c], T. Beau [d], A. de Bellefon [d], G. Bellini [e,6], J. Benziger [f], S. Bonetti [e], C. Buck [g], B. Caccianiga [e], L. Cadonati [f], F. Calaprice [f], G. Cecchet [c], M. Chen [h], A. Di Credico [b,10], O. Dadoun [d,2], D. D'Angelo [i,10], A. Derbin [j,1], M. Deutsch [k,5], F. Elisei [l], A. Etenko [m], F. von Feilitzsch [i], R. Fernholz [f], R. Ford [f,8], D. Franco [e], B. Freudiger [g,2,10], C. Galbiati [f,10], F. Gatti [n], S. Gazzana [b,10], M.G. Giammarchi [e], D. Giugni [e], M. Goeger-Neff [i], A. Goretti [b,10], C. Grieb [i], C. Hagner [a], E. Harding [f], G. Heusser [g], A. Ianni [b,10], A.M. Ianni [f,10], H. de Kerret [d], J. Kiko [g], T. Kirsten [g], V. Kobychev [b,3], G. Korga [e,4], G. Korschinek [i], Y. Kozlov [m], D. Kryn [d], M. Laubenstein [b,9], C. Lendvai [i,2,10], P. Lombardi [e,10], I. Machulin [m], S. Malvezzi [e], J. Maneira [h], I. Manno [o], D. Manuzio [n], G. Manuzio [n], F. Masetti [l], A. Martemianov [m,5], U. Mazzucato [l], K. McCarty [f], E. Meroni [e], L. Miramonti [e], M.E. Monzani [e], P. Musico [n], L. Niedermeier [i,2,10], L. Oberauer [i], M. Obolensky [d], F. Ortica [l], M. Pallavicini [n,10], L. Papp [e,4], L. Perasso [e], A. Pocar [f,10], R.S. Raghavan [p], G. Ranucci [e,7], A. Razeto [b], A. Sabelnikov [e], C. Salvo [n,8], R. Scardaoni [e], D. Schimizzi [f], S. Schoenert [g], H. Simgen [g], T. Shutt [f], M. Skorokhvatov [m], O. Smirnov [j], A. Sonnenschein [f], A. Sotnikov [j], S. Sukhotin [m], V. Tarasenkov [m], R. Tartaglia [b], G. Testera [n], D. Vignaud [d], S. Vitale [n,5], R.B. Vogelaar [a], V. Vyrodov [m], M. Wojcik [q], O. Zaimidoroga [j], G. Zuzel [q]

[a] *Virginia Polytechnic Institute and State University Blacksburg, VA 24061-0435, USA*
[b] *LNGS SS 17 bis Km 18+910, I-67010 Assergi (AQ), Italy*
[c] *Dipartimento di Fisica Nucleare e Teorica Università di Pavia, Via A. Bassi 6, I-27100 Pavia, Italy*
[d] *Laboratoire de Physique Corpusculaire et Cosmologie, 11 place Marcelin Berthelot, 75231 Paris Cedex 05, France*
[e] *Dipartimento di Fisica Università di Milano, Via Celoria 16, I-20133 Milano, Italy*
[f] *Department of Physics, Princeton University, Jadwin Hall, Washington Rd, Princeton, NJ 08544-0708, USA*
[g] *Max-Planck-Institut fuer Kernphysik, Postfach 103 980, D-69029 Heidelberg, Germany*
[h] *Department of Physics, Queen's University, Stirling Hall, Kingston, ON K7L 3N6, Canada*
[i] *Technische Universitaet Muenchen, James Franck Strasse E15, D-85747 Garching, Germany*
[j] *Joint Institute for Nuclear Research, 141980 Dubna, Russia*
[k] *Department of Physics, Massachusetts Institute of Technology, Cambridge, MA 02139, USA*
[l] *Dipartimento di Chimica, Università di Perugia, Via Elce di Sotto 8, I-06123 Perugia, Italy*
[m] *RRC Kurchatov Institute, Kurchatov Sq. 1, 123182 Moscow, Russia*
[n] *Dipartimento di Fisica Università and INFN Genova, Via Dodecaneso 33, I-16146 Genova, Italy*
[o] *KFKI-RMKI, Konkoly Thege ut 29-33, H-1121 Budapest, Hungary*
[p] *Bell Laboratories, Lucent Technologies, Murray Hill, NJ 07974-2070, USA*
[q] *M. Smoluchowski Institute of Physics, Jagellonian University, PL-30059 Krakow, Poland*

0370-2693/03/$ – see front matter
doi:10.1016/S0370-2693(03)00579-3

Received 6 August 2002; received in revised form 7 March 2003; accepted 11 April 2003
Editor: V. Metag

Abstract

The results of background measurements with the prototype of the Borexino detector (CTF) have been used to obtain an upper bound on the neutrino magnetic moment, μ_ν. The new upper limit for μ_ν from pp and ^{7}Be solar neutrinos is $(5.5\times10^{-10})\mu_B$ (90% c.l.) in the Standard Solar Model scenario. This is the first limit on μ_ν obtained using sub-MeV neutrinos. The sensitivity of the prototype to the neutrino charge radius and the neutrino radiative decay are also presented.

PACS: 14.60.S; 96.60.J; 26.65; 13.10

Keywords: Solar neutrinos; Charge radius; Magnetic moment

1. Introduction

The Lorentz-covariant total electromagnetic current for fermions can be presented in the following form [1]:

$$J_\alpha(q) = F(q^2)\gamma_\alpha + G(q^2)\big(q^2\gamma_\alpha - 2i(q_\alpha)\big)\gamma_5 + M(q^2)\sigma_{\alpha,\beta}q_\beta + iE(q^2)\sigma_{\alpha,\beta}q_\beta\gamma_5, \quad (1)$$

where q is the energy–momentum transfer to the fermion and the functions $F(q^2)$, $G(q^2)$, $M(q^2)$ and $E(q^2)$ are usually referred to as the electromagnetic, anapole, magnetic and electric dipole form factors, respectively. In the limit $q\to0$, F is the fermion electric charge, M is the dipole magnetic moment and E the electric dipole moment of the fermion. In the following we discuss the existing limits on the above electromagnetic form factors for neutrinos.

Assuming electric charge conservation in neutron decay $n\to p+e^-+\bar\nu_e$, experimental measurements of the $p+e^-$ [2] and n [3] charge lead to the upper limit $|e_{\bar\nu_e}|\leqslant10^{-21}e$. From astrophysical considerations, including solar and SN1987A data, the limits on the neutrino charge are less stringent $e_\nu\leqslant(10^{-13}-10^{-17})e$ [4,5].

The charge radius of the neutrino

$$\langle r^2\rangle \simeq 6\frac{\delta F(q^2)}{\delta q^2}\bigg|_{q^2=0}$$

(as well as the anapole moment for the Majorana neutrino) is induced by radiative corrections in the Standard Model of electroweak interactions (SM) and has a value equal to

$$\frac{G_F}{2\sqrt2\pi^2}\ln\frac{M_W^2}{m_e^2}\sim3.2\times10^{-33}\ \text{cm}^2$$

for the electron neutrino [6,7]. Modern accelerator experiments studying ν_μ–e scattering have sensitivity a few times poorer than needed to see the effect of these radiative corrections. The charge radius of the electron and muon neutrino has a bound of $-2.97\times10^{-32}\leqslant\langle r^2\rangle\leqslant4.14\times10^{-32}$ cm^2 [8,9] and $|\langle r^2\rangle|\leqslant6\times10^{-33}$ cm^2 [10,11], respectively.

The neutrino magnetic moment $\mu_\nu=M(0)$ in the SM is proportional to the neutrino mass. The value of μ_ν is

$$\mu_\nu=\frac{3m_eG_F}{4\pi^2\sqrt2}m_\nu\mu_B\approx3.2\times10^{-19}\left(\frac{m_\nu}{1\ \text{eV}}\right)\mu_B, \quad (2)$$

E-mail addresses: derbin@mail.pnpi.spb.ru (A. Derbin), osmirnov@jinr.ru (O. Smirnov).

[1] On leave of absence from St. Petersburg Nuclear Physics Inst., Gatchina, Russia.

[2] Marie Curie fellowship at LNGS.

[3] On leave of absence from Institute for Nuclear Research, MSP, 03680 Kiev, Ukraine.

[4] On leave of absence from KFKI-RMKI, Konkoly Thege ut 29-33, H-1121 Budapest, Hungary.

[5] Deceased.

[6] Spokesman.

[7] Project manager.

[8] Operational manager.

[9] GLIMOS.

[10] Task manager.

where μ_B is the electron Bohr magneton. The current 95% c.l. upper limit on the neutrino mass is 2.2 eV [12, 13], hence the neutrino magnetic moment calculated in the SM is less than $10^{-18}\mu_B$. A nonzero neutrino electric dipole moment, $d_\nu = E(0)$, is CP violating and, up to now, such a moment has not been observed for any particle. Both dipole moments, (μ_ν, d_ν), are forbidden for Majorana neutrinos in the case of CPT-invariance.

Since the mid 80s, the neutrino magnetic moment hypothesis has been widely discussed in the context of astrophysics. The solar neutrino flux measured by the Cl–Ar detector (Homestake) seemed to show a significant time variation in correlation with the solar magnetic activity as reported in [14–16]. It was shown [17–19] that this correlation could be caused by the interaction of the neutrino magnetic moment with the magnetic field in the convective zone of the Sun. This interaction leads to a flip of the neutrino helicity converting left-handed neutrinos into right-handed ones, which are not participating in the charged-current reactions in the detector. The value of the magnetic moment required for the observation of such variations with the present operating solar neutrinos detectors lies in the range of $(10^{-10}$–$10^{-11})\mu_B$. At present Homestake data are still analyzed to search for the mentioned time variations [20–22].

The so-called resonant spin-flavor precession (RSFP) of solar neutrinos due to the interaction of their transition magnetic moments with the solar magnetic field provides a suitable solution to the solar neutrino problem with $\mu_\nu \simeq 10^{-11}\mu_B$ [23–27].

The value of $10^{-10}\mu_B$ is eight orders of magnitude higher than the value predicted by the SM, but does not contradict the limit obtained in laboratory experiments. The elastic scattering of a neutrino by an electron turns out to be the most sensitive reaction to search for a nonzero neutrino magnetic moment. The measured cross sections for this process set the restriction $\mu_{\bar{\nu}_e} \leqslant (1.8 \times 10^{-10})\mu_B$ on a possible magnetic moment for electron antineutrinos [28,29],[11] $\mu_{\nu_e} \leqslant (1.1 \times 10^{-9})\mu_B$ for electron neutrinos [8], $\mu_{\nu_\mu} \leqslant (6.8 \times 10^{-10})\mu_B$ for muon neutrinos [8] and $\mu_{\nu_\tau} \leqslant (3.9 \times 10^{-7})\mu_B$ for tau neutrinos [33].

The most stringent limits on the neutrino magnetic moment in the range of $(10^{-12}$–$10^{-10})\mu_B$ come from astrophysical observations. These limits are based mainly on the fact that the scattering of neutrinos with a large magnetic moment by charged particles would lead to an intensive production of right-handed neutrinos that do not participate in weak interactions, and hence change the dynamics of stars. The observation of neutrinos formed as a result of a supernova burst, SN1987A, has led to the limit of $10^{-12}\mu_B$ ([4,5] and references therein). As far as solar neutrinos are concerned, an upper bound for a magnetic moment using ^{8}B neutrinos was obtained in [34], $\mu_\nu \leqslant (2.2$–$2.3) \times 10^{-10}\mu_B$ using data from Super-Kamiokande, Kamiokande and Homestake. A more recent analysis of the Super-Kamiokande ^{8}B data sets an upper limit on the neutrino magnetic moment at the level of $(1.5 \times 10^{-10})\mu_B$ (90% c.l.) [35]. Bounds on the elements of the neutrino magnetic moment tensor of the order of some units of $10^{-10}\mu_B$ were obtained from solar neutrinos data in [36,37]. From Super-Kamiokande and SNO data the charge radius is limited at values $\leqslant 6.9 \times 10^{-32}$ cm^2 [36]. Moreover, from the same data, taking into account that μ_ν and $\langle r^2 \rangle$ are correlated, it is found: $-1.2 \times 10^{-32} \leqslant \langle r^2 \rangle \leqslant 2.7 \times 10^{-32}$ cm^2, when $\mu_\nu = 0$ for Dirac neutrinos [38].

From the above discussion one can see that the existing experimental bounds are far from the value predicted by the SM. However, in models with right-handed bosons or with an extended sector of scalar particles, the magnetic moment can be proportional to the mass of intermediate leptons and can have values at the level of the experimental limits reported [39,40].

In this Letter we present the limits on the neutrino magnetic moment, charge radius and neutrino radiative decay life time obtained for the first time in the sub-MeV neutrino region with a Borexino prototype. The preliminary results were reported in [41].

2. The experimental setup and the results of measurements

Borexino, a real-time detector for low energy neutrino spectroscopy, is near completion in the under-

[11] Recently [30], a preliminary result for limit on μ_ν for the reactor $\bar{\nu}_e$ at the level of $(1.3$–$1.7) \times 10^{-10}\mu_B$ has been reported by the MUNU [31] and TEXONO [32] Collaborations.

ground laboratory at Gran Sasso (see [42] and references therein). The main goal of the detector is the direct measurement of the flux of ^{7}Be solar neutrinos via neutrino–electron scattering in an ultra-pure liquid scintillator. Borexino will also address several other frontier questions in particle physics, astrophysics and geophysics.

2.1. The counting test facility detector

The counting test facility (CTF) of the Borexino detector was constructed in Hall C of the Gran Sasso Laboratory. The main goal of the CTF was to test the key concept of Borexino, namely the possibility to purify a large mass of liquid scintillator at a level of contamination in U and Th of a few times 10^{-16} g/g. This goal was successfully achieved with the first prototype (CTF-I, [43]) operated in 1995–1997. The detector was reinstalled in 1999 (CTF-II, [44]) with the purpose of serving as a facility for the quality control of the pseudocumene to be delivered for the Borexino experiment. Although the CTF is a large-scale detector (4 tons of liquid scintillator), its size is nonetheless modest in comparison to Borexino (300 tons). A mass in the 4-ton range was set by the need to make the prevailing scintillator radioimpurities measurable via delayed coincidence tagged events in the decay chains of U/Th and in the β decay of ^{85}Kr. The primary goal of the CTF was test of the design and purification issues for Borexino; in the future there will be also the long-range goal of performing quality control during Borexino operations. Detailed reports on the CTF have been published [42–47].

As a simplified, scaled version of the Borexino detector, the CTF contains a volume of liquid scintillator in a 2 m diameter transparent inner nylon vessel mounted at the center of an open structure that supports 100 phototubes (PMT) [48] which detect the scintillation signals. The whole system is placed within a cylindrical tank (11 m in diameter and 10 m height) that contains 1000 tons of ultra-pure water, which provide 4.5 m of shielding against neutrons originating from the rock and against external γ rays from PMTs and other construction materials. The scintillator used for the major part of tests in the CTF-I was a binary mixture consisting of pseudocumene (PC, C_9H_{12}) as a solvent and 1.5 g/L of PPO (2,5-diphenyloxazole) as a fluor. The CTF-II data analyzed in the present Letter were acquired with an alternate liquid scintillator solvent, phenylxylylethane (PXE, $C_{16}H_{18}$).[12] The scintillator was carefully purified to ensure the ^{238}U and ^{232}Th in it were less than 10^{-15} g/g. The PMTs are 8-inch diameter ETL 9351 tubes made of low radioactivity glass and characterized by high quantum efficiency (26% at 420 nm), limited transit time spread (1 ns) and good pulse height resolution for single photoelectrons (Peak/Valley = 2.5). The number of photoelectrons registered by one PMT for a 1 MeV energy deposit at the detector's center is about 3.5 for the PXE.

2.2. Response function of the CTF-II detector

The energy of an event in the CTF detector is defined using the total collected charge from all PMTs. In a simple approach the energy is supposed to be linear with respect to the total collected charge. The coefficient linking the event energy and the total collected charge is called the light (or photoelectron) yield. The light yield for electrons can be considered linear with respect to its energy only for energies above 1 MeV. At low energies the phenomenon of "ionization quenching" violates the linear dependence of the light yield versus energy [49]. The deviations from the linear law can be taken into account by the ionization deficit function $f(k_B, E)$, where k_B is Birks' constant. For the calculations of the ionization quenching effect for PXE scintillator we used the KB program from the CPC library [50].

Because of this nonlinear dependence of the light yield versus energy released, due to the ionization quenching effect, the CTF resolution should be expressed in terms of the total registered charge, which is directly measured in the experiment.

A study with the radioactive sources placed at different positions inside the CTF inner vessel showed that the CTF response can be approximated by a Gaussian with sigma defined by the following formula:

$$\sigma_Q = \sqrt{(1+\overline{v}_1)Q + v_p Q^2}, \tag{3}$$

[12] With p-diphenylbenzene (para-terphenyl) as a primary wavelength shifter at a concentration of 2 g/L along with a secondary wavelength shifter 1,4-bis-(2-methylstyrol)-benzene (bis-MSB) at 50 mg/L.

where

- $Q = AEf(k_B, E)v_f$ is the mean total registered charge for events of energy E distributed over the detector's volume;
- $\bar{v}_1 = \frac{1}{N_{\rm PM}} \sum_{i=1}^{N_{\rm PM}} s_i v_{1_i}$ is the relative variance of the PMT single photoelectron charge spectrum (v_{1_i}) averaged over all PMTs ($N_{\rm PM}$), taking into account the ith PMTs relative sensitivity s_i ($\bar{v}_1 = 0.34$);
- A is the scintillator specific light yield measured in photoelectrons per MeV ($A = 350$ p.e./MeV in CTF-II for events at the detector's center);
- v_f is the volume factor, coming from averaging the signals over the CTF volume ($v_f \equiv \langle Q \rangle_V / Q_0 = 1.005$);
- v_p is the parameter which takes into account the variance of the signal for a source uniformly distributed over the detector's volume ($v_p \equiv (\langle Q^2 \rangle_V - \langle Q \rangle_V^2)/Q_0^2 = 0.0023$). This parameter gives additional signal variance for a source distributed over the detector's volume in comparison to a point-like source at the detector's center. This last case will naturally yield $v_p = 0$ (and $v_f = 1$).

All the parameters in (3) were defined with satisfactory precision from the CTF-II data (see [51,52] for the details). The radial dependence of the detector response was defined from the experimental data as well.

For the energy resolution one can use the approximation $\sigma_E/E \approx \sigma_Q/Q$.

2.3. Data selection and residual background modeling

In our analysis we used data from CTF-II with 32.1 days of data taking (see Fig. 1). Muon identification cuts remove most of the background induced by muons (more details on the muon veto can be found in [44]). The remaining background is shown in Fig. 1 (line B). Although the absolute number of muons events is higher at low energies, the relative reduction by the cut is more pronounced at high energies. Pulse shape analysis was employed to distinguish signals caused by electrons and α particles. Line C in Fig. 1 shows the remaining, predominantly electron-like background.

The major part of the CTF background in the energy region up to 200 keV is induced by the β activity of ^{14}C. Another relatively strong source of background is the soft part of the β and γ spectra coming from the decay of ^{40}K present in the detector construction materials (the decays occur outside of the scintillator volume).

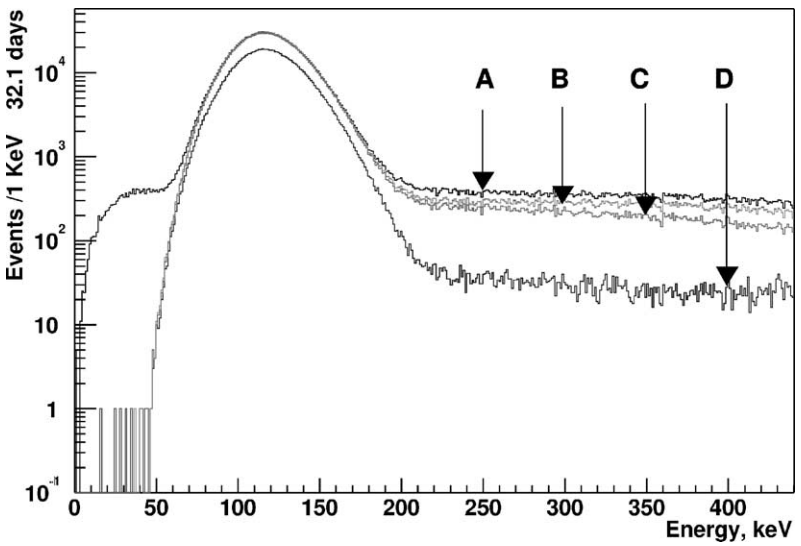

Fig. 1. The CTF-II background in the low energy region and the result of the sequential cuts applied in order to reduce background: (A) raw data; (B) muons cut; (C) (α/β) discrimination; (D) radial cut (with $R = 100$ cm).

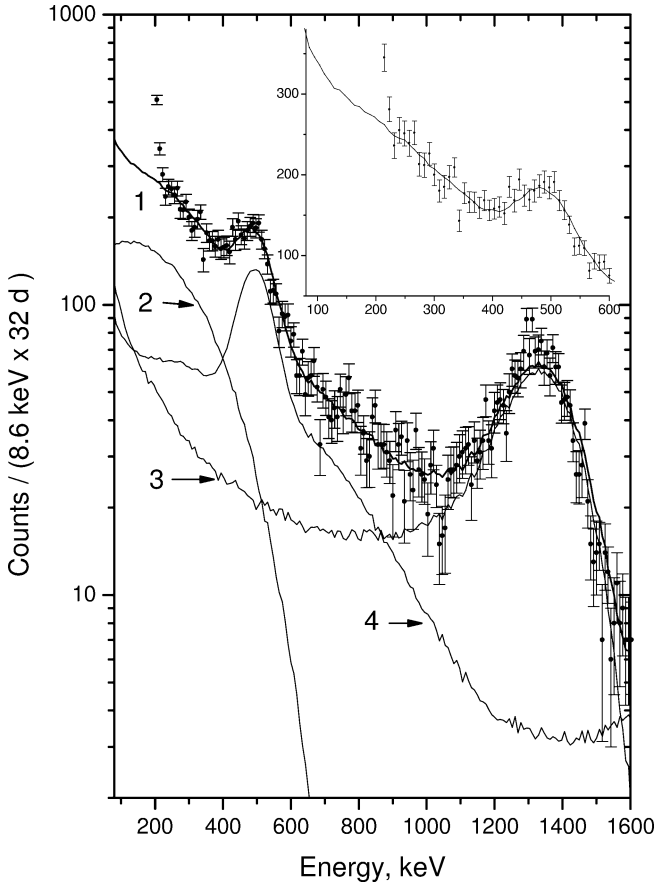

Fig. 2. The fit (line 1) of the CTF-II data (points with error bars) performed to study the behaviour of the background in the range 100–400 keV. The background is mainly due to internal ^{39}Ar and ^{85}Kr (line 2); external ^{40}K (line 3); internal and external ^{222}Rn and ^{238}U–^{232}Th chain (line 4). The response functions (1)–(4) are calculated with the Monte Carlo method. The shift in the position of the full absorption peak of the 1.46 MeV ^{40}K γ's is due to the ionization quenching effect (see Section 2).

An analysis has been performed, showing that the source of ^{40}K is outside the inner vessel [44]. It shows that most of the ^{40}K events can be removed by applying a radial cut on the reconstructed event position (see [46] for the details of the reconstruction code). A study to look for best radial cut has been performed, varying the radius from $R = 90$ cm to $R = 110$ cm. The final goal was to provide maximal surface background reduction with a minimal loss of the ^{14}C events uniformly distributed over the detector's volume. It was found that the best ratio between the background reduction and detector's effective volume is achieved at $R = 100$ cm. Using this cut, a background reduction of a factor of about 8 in the energy region around 250 keV was achieved. At the same time only about 30% of the ^{14}C spectrum is lost in the region of interest (line D in Fig. 1).

The remaining electron background at the region 250–450 keV of ~ 0.07 counts/(keV kg yr) is the lowest value achieved in large-scale, low-background installations.

The residual background is practically linear in the region 220–450 keV, and one can expect the same linear behaviour down to the lower limit used. A detailed Monte Carlo simulations of the detector's backgrounds were performed taking into account all possible contributions from ^{238}U, ^{232}Th, ^{40}K, ^{39}Ar and ^{85}Kr in the scintillator, from ^{238}U, ^{232}Th and ^{40}K in the surrounding water and in the inner vessel material. In Fig. 2 we show the result of the CTF-II background

Table 1
The results of the fit before and after the radial cut (RC) applied. One can see that the parameters responsible for the ^{14}C spectrum shape (A, k_B and α) remains unchanged within their errors

Par	χ^2	N_0	A	k_B	α	a	b
Before RC	$\frac{325}{306}$	$(1.79 \pm 0.02) \times 10^7$	372 ± 8	$(1.5 \pm 0.1) \times 10^{-3}$	-0.55 ± 0.3	360 ± 15	-1.47 ± 0.05
After RC	$\frac{317}{306}$	$(1.22 \pm 0.01) \times 10^7$	373 ± 7	$(1.5 \pm 0.1) \times 10^{-3}$	-0.75 ± 0.4	53.6 ± 2.5	-0.24 ± 0.01

fit using the Monte Carlo data. It should be noted a good agreement of the fit with experimental data in the energy window 230–2300 keV ($\chi^2 = 284/237$ d.o.f.). The shape of the background underlying the ^{14}C β spectrum has a linear behaviour with a negative slope for energies between 100 and 400 keV (see inset in Fig. 2).

The residual background at low energies is dominated by the ^{14}C β spectrum, but its shape is significantly effected by the detector efficiency at $E \simeq 130$ keV. The part of the spectrum starting at 138 keV has been used for the residual background modeling, in order to avoid the spectrum distortions caused by the mentioned effect. The efficiency was estimated with Monte Carlo, taking into account the spatial distribution of the events, the electronics threshold and the map of working PMTs. More details on the threshold effect can be found in [51].

The β decay of ^{14}C is an allowed ground state to ground state ($0^+ \to 1^+$) Gamow–Teller transition with an endpoint energy of $E_0 = 156$ keV and half-life of 5730 years. The ^{14}C spectrum in the CTF detector was studied in detail in [45]. The deviations from the allowed shape of the ^{14}C spectrum are usually parametrized as $C(E) = 1 + \alpha E$. Although the β decay of ^{14}C has been investigated by many groups over almost 50 years, the situation with the shape factor is still unclear [53]. Therefore, we leave this parameter free in our estimations. The procedure for fitting the ^{14}C spectrum is described in detail in [51].

The model function for the residual background can be written as the sum of the ^{14}C spectrum S^β and the polynomial for the underlying background

$$S^{\text{Model}}(Q) = N_0 S^\beta\big(Q, \{A, k_B, \alpha\}\big) + a + bQ, \qquad (4)$$

with 6 free parameters:

- N_0 is the number of ^{14}C decays;
- A is scintillator light yield measured in p.e./MeV;
- k_B is quenching factor;
- α is ^{14}C shape factor (MeV^{-1});
- a, b are the parameters describing the linear background underlying the residual spectrum.

The endpoint energy of the ^{14}C spectrum has been measured in other experiments with sufficient accuracy $E_0 = (156 \pm 0.5)$ keV and was fixed in our calculations. The endpoint energy is strongly correlated with the energy scale parameter A and there is no need to free both parameters in the fit.

The χ^2 method was used to find the best values for the free parameters of the model function,

$$\chi^2 \equiv \sum_i \frac{(S_i^{\text{Model}} - S_i^{\text{Exp}})^2}{S_i^{\text{Model}}},$$

where S_i^{Exp} and S_i^{Model} are the contents of the ith bin of the experimental histogram and the corresponding model value, respectively. The analysis of the CTF-II spectrum for 32.1 days of data in the energy region 138–420 keV before and after the radial cut (RC) are shown in Table 1. The comparison of the parameters leads to the conclusion that the shape of the spectrum is not influenced by the radial cut applied. The ratio of the values of the N_0 parameter before and after the radial cut gives us an efficiency of the RC of $\epsilon = 0.67$ for events uniformly distributed over the detector volume.

The error estimate for each parameter was defined by analyzing the behaviour of the $\chi^2(N_0, A, k_B, \alpha, a, b)$ function using the following algorithm. First, a set of equidistant values of the parameter was chosen in a wide interval around the best-fit value of the same parameter. Then, for each parameter value from the set, the minimum of the χ^2 was found leaving the remaining 5 parameters free. The increase of χ^2 by one unit with respect to χ^2_{min} gives the one standard deviation interval for the parameter under consideration.

The value of the parameters A and k_B agree with values obtained from separate measurements made with a radon source; the range of values for α is not ruled out by existing experiments. The large uncertainty in the parameters α and k_B reflects the fact that the corrections caused by these two parameters are small in the analyzed region ($E > 138$ keV), and that they are anticorrelated.

3. Analysis

3.1. Neutrino–electron elastic scattering

Neutrino–electron elastic scattering is the most sensitive test for a neutrino magnetic moment search. In the SM, the scattering of a neutrino with a nonzero magnetic moment is determined both by a weak interaction term and by a one-photon exchange contribution. The latter changes the helicity of the final neutrino state. Therefore, the amplitudes of the weak and electromagnetic scattering do not interfere, at least at the level of $\sim m_\nu/E_\nu$, and the total cross section is the sum of the two cross sections.

The differential cross section for the weak contribution to neutrino–electron elastic scattering has the form:

$$\frac{d\sigma_W}{dT_e}(T_e, E_\nu) = 4\sigma_0\left[g_L^2 + g_R^2\left(1 - \frac{T_e}{E_\nu}\right)^2 - g_L g_R \frac{T_e m_e}{2E_\nu^2}\right], \quad (5)$$

where $\sigma_0 = \frac{G_F^2 m_e}{2\pi} = 4.28 \times 10^{-45}$ cm^2/MeV, the values of g_R and g_L depend only on the Weinberg angle ($\sin^2\theta_W = 0.2315$) with $g_L = g_V + g_A = \frac{1}{2} + \sin^2\theta_W$, $g_R = g_V - g_A = \sin^2\theta_W$, and E_ν and T_e are the energies of the incident neutrino and the recoil electron. The scattering due to a charge radius interferes with the weak scattering contribution. In this case the parameters g_R and g_L are modified in accordance with a new value of $g'_V = g_V + x$, where $x = \frac{\sqrt{2}\pi\alpha}{3G_F}\langle r^2\rangle = 2.38 \times 10^{30}\langle r^2\rangle$ cm^2.

The ν–e scattering cross section associated with the magnetic moment is

$$\frac{d\sigma_{\mu_\nu}}{dT_e}(T_e, E_\nu) = \pi r_0^2 \mu_\nu^2\left(\frac{1}{T_e} - \frac{1}{E_\nu}\right), \quad (6)$$

where μ_ν is an effective neutrino magnetic moment measured in μ_B units, and $r_0 = 2.818 \times 10^{-13}$ cm is the classical electron radius. We analyzed our data in the assumption that the cross section is described by Eq. (6).

In case of neutrino mixing μ_ν^2 is given by [35,36]

$$\mu_\nu^2 = \sum_j \left|\sum_k \mu_{jk} A_k(E, L)\right|^2, \quad (7)$$

where μ_{jk} is the fundamental matrix which characterizes the neutrino electromagnetic coupling; $A_k(E, L)$ is the probability amplitude of the neutrino mass eigenstate ν_k at the detector, if produced in the sun core as ν_e. In the general case μ_ν^2 might depend not only on the mixing angles but also on the neutrino energy and source-detector distance L. For the vacuum oscillations $A_k(E, L) = U_{ek} e^{-iE_k L}$, where U_{ek} is an element of the mixing matrix.[13] With reasonable assumptions in the case of vacuum oscillations μ_ν^2 has no dependence on L and E_ν and depends only on μ_{jk} and vacuum mixing U_{ek}. In particular, for Dirac neutrinos: $\mu_\nu^2 = \sum_{k=1}^3 |U_{ek}|^2 |\mu_{kk}|^2$. On the contrary, for Majorana neutrinos and assuming only two relevant mass eigenstates, $\mu_\nu^2 = |\mu_{12}|^2$ [35].

If the neutrino flavor conversion is caused by the MSW mechanism then the probability amplitude $A_k(E, L)$ is defined by the mixing angle in the sun matter. The former depends on $\delta m^2/E_\nu$. For three light neutrinos, the effective magnetic moment is [35–37]

$$\mu_\nu^2 = P_{e1}\mu_{11}^2 + (1 - P_{e1})\mu_{22}^2 + \mu_{12}^2 + P_{e1}\mu_{13}^2 + (1 - P_{e1})\mu_{23}^2, \quad (8)$$

where $P_{e1} = |A_1(E, L)|^2$ is the probability of the $\nu_e \to \nu_1$ transition after crossing the resonant point. Since the expression for μ_ν^2 contains a sum of positive terms one can set upper bounds on each μ_{jk} (except μ_{33}) using the upper limit on μ_ν^2 and P_{e1} value. Recently, the KamLAND Collaboration [56] has provided further experimental data in favour of the LMA solution to the solar neutrinos puzzle. The LMA solution gives P_{e1} close to 0.5 in the case of Borexino (sub-MeV neutrinos). As follows from Eq. (8), this value

[13] The weak "interaction eigenstates", ν_l ($l = e, \mu, \tau$), are related to the mass eigenstates, ν_i, by virtue of a unitary mixing matrix, U: $\nu_l = \sum_{i=1}^3 U_{li}\nu_i$.

is optimal to constrain the sum of transition moments $\mu_{12}^2 + \mu_{23}^2 + \mu_{13}^2$ for Majorana neutrinos [37] and diagonal magnetic moments $\mu_{11}^2 + \mu_{22}^2$ for Dirac neutrinos. This fact, together with a low threshold for the recoil electrons (250 keV), makes Borexino substantially more sensitive to the search for the solar neutrino magnetic moment than any of the existing experiments.

The energy dependence of the cross sections for the magnetic and weak scattering differs significantly; for $T_e \ll E_\nu$ their ratio is proportional to $1/T_e$, i.e., a decrease of the electron detection threshold will increase the sensitivity of the experiment to the magnetic moment.

To get the expected energy spectrum of the recoil electrons in the detector it is necessary to fold the cross sections (5) and (6) with the neutrino spectrum, $\phi_\nu(E)$:

$$\frac{dN}{dT_e}(T_e) = \int_{E_{\nu\min}(T_e)}^{E_{\nu\max}} \frac{d\sigma}{dT_e}(T_e, E_\nu)\phi_\nu(E_\nu)\,dE_\nu. \tag{9}$$

In this expression, $E_{\nu\min}(T_e) = \frac{T_e}{2}(1+\sqrt{1+2m_e/T_e})$, is the minimum energy of the neutrino at which a recoil electron with an energy T_e can be generated.

In the calculations we used the neutrino fluxes given by the Standard Solar Model (SSM) [54] and neutrino energy spectra from [55]. The signal shapes (9) were convoluted with the detector response function

$$S(Q) = N_e T \varepsilon \int \frac{dN}{dT_e}\big(T_e(Q')\big)\frac{dT_e}{dQ}\,\mathrm{Res}(Q, Q')\,dQ', \tag{10}$$

where $\mathrm{Res}(Q, Q') = \frac{1}{\sqrt{2\pi}\sigma_Q} e^{-\frac{1}{2}((Q-Q')/\sigma_Q)^2}$ is the detector response function, σ_Q is defined by (3).

The expected spectra for the SSM neutrino weak contribution, $S^W(Q)$, and the magnetic one, $S^{\mu_\nu}(Q)$ (for $\mu_\nu = 10^{-9}\mu_B$) are shown in Fig. 3. The spectra are calculated in accordance with (4) using the cross sections (5) and (6) for the total number of target electrons in CTF-II $N_e = 1.36 \times 10^{30}$, the time of data taking $T = 32.1$ days, and an efficiency $\varepsilon = 0.67$ defined by the spatial cut applied and with the dead time of the electronics subtracted. The weak interaction contribution was not taken into account because it is more than one order of magnitude less than the limit from the electromagnetic contribution (see Fig. 3).

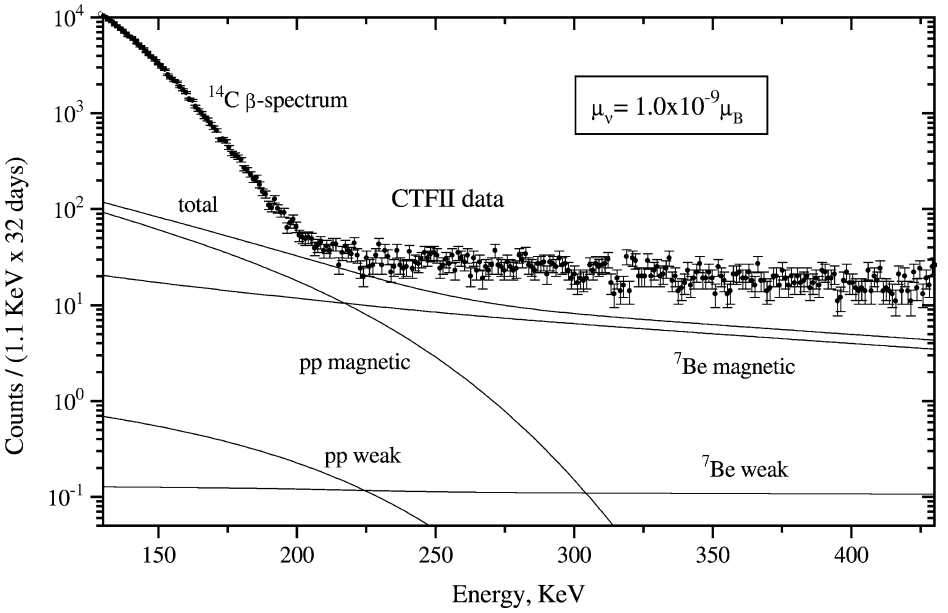

Fig. 3. The experimental spectrum measured by the CTF-II (upper plot with error bars) and the expected spectra for magnetic and weak scattering of *pp* and (^{7}Be) neutrinos calculated in accordance with (5)–(6), (9)–(10).

3.2. Upper limit on the neutrino magnetic moment

If the total rate in the energy region around 220 keV in Fig. 3 would be attributed to the neutrino magnetic scattering, then a conservative estimate of the neutrino magnetic moment is $\mu_\nu = (1.2 \times 10^{-9})\mu_B$. In our analysis we used the different energy dependence of the background spectrum and the spectrum of the recoil electrons due to the magnetic scattering. An analysis interval of 185–380 keV was chosen to select the region with maximal statistical significance of the expected effect while minimizing the additional systematic uncertainties related to the linear background that increases at lower energies.

The α, k_B and A parameters were fixed in the analysis at the values found during the data fitting in the high statistics region of 138–420 keV; the other three parameters were free. Changes in α and k_B do not significantly influence the results of this analysis; the parameter A is also well established experimentally, from separate measurements with a radon source.

An analysis of the upper limit for a possible magnetic moment of the neutrino was performed minimizing the

$$\chi^2\left(N_0, a, b, \mu_\nu^2\right) \equiv \sum \frac{(S_i^{\text{Model}} + S_i^{\mu_\nu} - S_i^{\text{Exp}})^2}{S_i^{\text{Model}} + S_i^{\mu_\nu}}$$

for different values of μ_ν^2. The minimum of the χ^2 corresponds to $\mu_\nu = (3.2 \times 10^{-10})\mu_B$. In order to define an upper limit for μ_ν, the probability function, $P(\chi^2(\mu_\nu^2))$, was renormalized to the physical region $\mu_\nu^2 \geqslant 0$, in accordance with the recommendations of the Particle Data Group [5]. The integration of the probability function gives 0.9 (90% c.l.) for $\mu_\nu = (5.5 \times 10^{-10})\mu_B$. This limit is practically independent of the lower bound of the analyzed energy region. The fit with an exponential underlying background gives slightly stronger limit on the $\mu_\nu = (5.0 \times 10^{-10})\mu_B$. So our limit is practically independent of the model chosen. The results of the best fit for $\mu_\nu = (5.5 \times 10^{-10})\mu_B$ are shown in Fig. 4. The neutrino magnetic moment of $\mu_\nu = (5.5 \times 10^{-10})\mu_B$ (excluded with 90% c.l.) would yield about 20% of the total background in the region 200–250 keV. This low 'signal to noise' sensitivity is explained by the similarity of the shapes of the background and the magnetic moment effect (linear function with

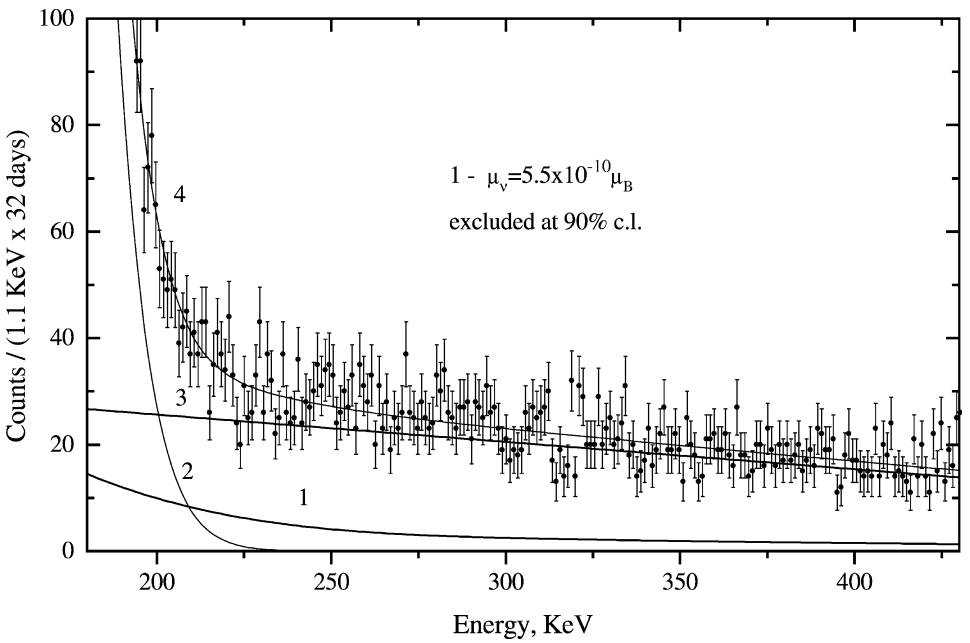

Fig. 4. The fit in the region 185–380 keV for $\mu_\nu = (5.5 \times 10^{-10})\mu_B$. (1) the spectrum of recoil electrons due to magnetic scattering; (2) ^{14}C β spectrum; (3) linear background; (4) total fit.

small negative slope), and by the impossibility to perform 'background only' measurements with the Sun 'switched off', as in the reactor experiments.

The limit obtained is only about 3 times worse compared to the 825-day Super-Kamiokande result [35], and is the first one obtained with sub-MeV neutrinos in a direct experiment. As one can see from Fig. 3 the limit on the magnetic moment with the Borexino detector will be improved by an order of magnitude when Borexino will achieve sensitivity for ^{7}Be neutrinos.

3.3. Other neutrino electromagnetic properties

We also analyzed the sensitivity of the CTF-II data to a potential neutrino charge radius. In accordance with (5) the energy spectrum of recoil electrons has the same shape as in the case of weak scattering. For this reason, the low energy threshold of the CTF-II offers no advantage in searching for a neutrino charge radius. The upper limit we obtained is $\langle r^2\rangle \leqslant 2.2 \times 10^{-30}$ cm^2 (90% c.l.). The expected spectrum of the recoil electrons for this value of the charge radius is shown in Fig. 5. The result is poorer than the one obtained in accelerator experiments [8–11] and with ^{8}B solar neutrinos [36,38]. It was also found that the sensitivity of the detector to the weakly interacting pp neutrinos is about 46 times the flux predicted by the SSM, i.e., $\phi(pp) \leqslant 46\phi_{\mathrm{SSM}}(pp)$ at 90% c.l. This should be compared to the results of the SAGE and GALLEX/GNO experiments of $0.58 \pm 0.04\ \phi_{\mathrm{SSM}}$, nevertheless our result is the first available using solar pp-neutrino detected in real-time.

If neutrinos have mass, then the heavier ones could decay to lighter ones $\nu_H \to \nu_L + \gamma$. A search for neutrino decay provides information about neutrino mass and mixing [57–61]. The CTF can detect the γ rays that appear in a neutrino radiative decay. The procedure for this analysis was the same as in the case of searching for a neutrino magnetic moment and has been described separately in [62]. Because this process is related to that which governs a possible neutrino magnetic moment, we give the limits here, derived from a likelihood function analysis at 90% c.l. (Fig. 5): $\tau_{\mathrm{c.m.}}/m_\nu > 4.2 \times 10^3$ s/eV ($\alpha = 0$), $\tau_{\mathrm{c.m.}}/m_\nu > 9.7 \times 10^3$ s/eV ($\alpha = 1$) and $\tau_{\mathrm{c.m.}}/m_\nu > 1.5 \times 10^3$ s/eV ($\alpha = -1$); here the parameter α defines the angular distribution of the photon, relative to the spin of the decaying neutrino in the neutrino rest frame, and relates to the space–time structure of the decay vertex.

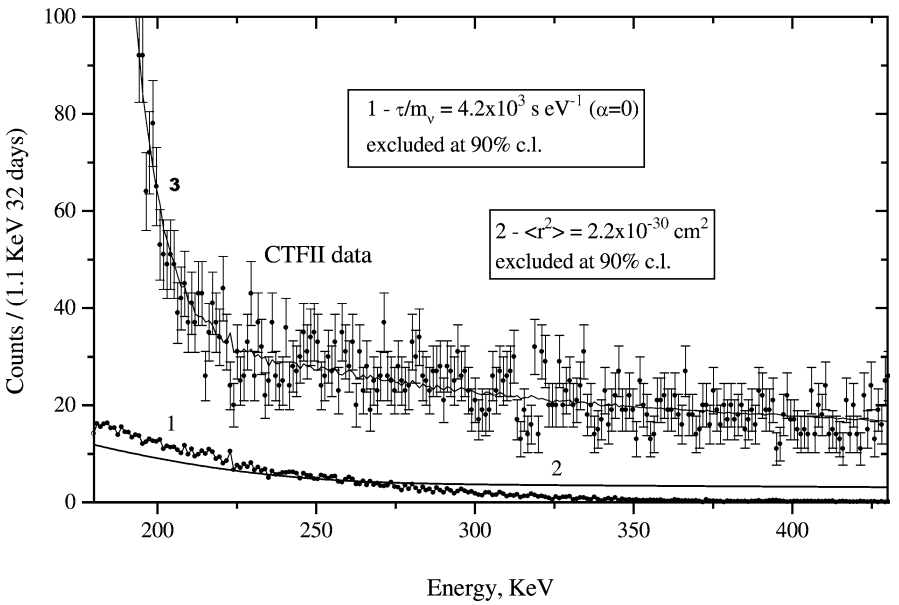

Fig. 5. The fit in the region 185–380 keV for radiative neutrino decay and ν_e–e scattering due to a charge radius. (1) Monte Carlo calculation of the γ signal from $\nu_H \to \nu_L + \gamma$ decay for $\tau/m_\nu = 4.2 \times 10^3$ eV^{-1}; (2) spectrum of recoil electrons for a neutrino charge radius $\langle r^2\rangle = 2.2 \times 10^{-30}$ cm^2.

This is more than one order of magnitude stronger than obtained in reactor and accelerator experiments [63–68], but is still poorer in comparison to the astrophysical considerations [69,70].

4. Conclusions

Although no solar neutrinos were observed in the Borexino prototype set-up, the outstanding background levels achieved provides limits on the electromagnetic properties of low-energy neutrinos. A new upper limit on the neutrino magnetic moment from pp and ^{7}Be solar neutrinos has been established, $\mu_\nu \leqslant (5.5 \times 10^{-10})\mu_B$ (90% c.l.), in the assumption of SSM neutrino fluxes. This value is only 3 times weaker then the one obtained from reactor neutrinos and using ^{8}B solar neutrinos. The upper limit for the charge radius is $\langle r^2 \rangle \leqslant 2.2 \times 10^{-30}$ cm^2 (90% c.l.). The low energy threshold of CTF has no essential advantages in searching for the charge radius, as it does in the case of the neutrino magnetic moment and neutrino radiative decay. The limit for the mean life time of pp and ^{7}Be neutrino radiative decay $\tau_{\text{c.m.}}/m_\nu > 4.2 \times 10^3$ s/eV is stronger than the one obtained in direct laboratory experiments. All these results are the first ones obtained using sub-MeV neutrinos.

The Borexino detector will improve the bounds on μ_ν at least by one order of magnitude and bounds on the charge radius and the mean life time of the neutrino radiative decay by roughly two orders of magnitude.

References

[1] B. Kayser, Phys. Rev. D 26 (1982) 1662.
[2] M. Marinelli, G. Morpurgo, Phys. Lett. B 137 (1984) 439.
[3] J. Baumann, et al., Phys. Rev. D 37 (1988) 3107.
[4] G.G. Raffelt, Phys. Rep. 320 (1999) 319.
[5] Particle Data Group, K. Hagiwara, et al., Phys. Rev. D 66 (2002) 010001.
[6] W.J. Marciano, A. Sirlin, Phys. Rev. D 22 (1980) 2695.
[7] P. Vogel, J. Engel, Phys. Rev. D 39 (1989) 3378.
[8] LSND Collaboration, L.B. Auerbach, et al., Phys. Rev. D 63 (2001) 112001.
[9] R.C. Allen, et al., Phys. Rev. D 47 (1993) 11.
[10] P. Vilain, et al., Phys. Lett. B 345 (1995) 115.
[11] L.A. Ahrens, et al., Phys. Rev. D 41 (1990) 3297.
[12] Ch. Weinheimer, in: Proceedings XXth International Conference on Neutrino Physics and Astrophysics, May 25–30, 2002, Munich, Germany, in press.
[13] V.M. Lobashev, et al., Phys. Lett. B 460 (1999) 227.
[14] G.A. Bazilevskaya, Ju.I. Stojkov, T.N. Charahchay, et al., JETP Lett. 35 (1982) 273.
[15] B.N. Gavrin, Ju.S. Kopusov, N.T. Makeev, JETP Lett. 35 (1982) 491.
[16] J.N. Bahcall, Neutrino Astrophysics, Cambridge Univ. Press, Cambridge, 1989.
[17] M.B. Voloshin, M.I. Vysotskii, Yad. Fiz. 44 (1986) 845.
[18] L.B. Okun', Yad. Fiz. 44 (1986) 847.
[19] M.B. Voloshin, M.I. Vysotskii, L.B. Okun', Yad. Fiz. 44 (1986) 677.
[20] G. Walther, Phys. Rev. Lett. 79 (1997) 4522.
[21] D.S. Oakley, et al., Astropys. J. 437 (1994) L63.
[22] P.A. Sturrock, G. Walther, M.S. Wheatland, Astrophys. J. 507 (1998) 978.
[23] E.Kh. Akhmedov, Yad. Fiz. 48 (1988) 599;
E.Kh. Akhmedov, Phys. Lett. B 213 (1988) 64.
[24] G.S. Lim, W.J. Marciano, Phys. Rev. D 37 (1988) 1368.
[25] J. Pulido, Phys. Rep. 211 (1992) 211, hep-ph/0106201;
J. Pulido, hep-ph/0101116.
[26] J. Pulido, E.Kh. Akhmedov, Astropart. Phys. 13 (2000) 227.
[27] E.Kh. Akhmedov, J. Pulido, Phys. Lett. B 485 (2000) 178;
E.Kh. Akhmedov, J. Pulido, Phys. Lett. B 529 (2002) 193.
[28] A.V. Derbin, Yad. Fiz. 57 (1994) 236;
A.V. Derbin, Phys. At. Nucl. 57 (1994) 222.
[29] G.S. Vidyakin, et al., JETP Lett. 55 (1991) 206.
[30] J. Vuilleumier, in: Proceedings XXth International Conference on Neutrino Physics and Astrophysics, May 25–30, 2002, Munich, Germany, in press.
[31] C. Broggini, et al., Nucl. Phys. B (Proc. Suppl.) 91 (2001) 105.
[32] TEXONO Collaboration, H.T.-K. Wong, hep-ex/0209003;
TEXONO Collaboration, H.T.-K. Wong, hep-ex/0212003.
[33] DONUT Collaboration, R. Schwienhorst, et al., Phys. Lett. B 513 (2001) 23.
[34] J. Pulido, A.M. Mourao, Phys. Rev. D 57 (1998) 1794.
[35] J.F. Beacom, P. Vogel, Phys. Rev. Lett. 83 (1999) 5222.
[36] A. Joshipura, S. Mohanty, hep-ph/0108018;
A. Joshipura, S. Mohanty, hep-ph/0204305.
[37] W. Grimus, et al., hep-ph/0208132.
[38] A. Ianni, Phys. Lett. B 540 (2002) 20.
[39] M.I. Voloshin, Yad. Fiz. 48 (1988) 804.
[40] M. Leurer, N. Marcus, Phys. Lett. B 237 (1990) 81.
[41] Borexino Collaboration, A. Derbin, O. Smirnov, in: Proceedings XXth International Conference on Neutrino Physics and Astrophysics, May 25–30, 2002, Munich, Germany, in press.
[42] Borexino Collaboration, G. Alimonti, et al., Astropart. Phys. 16 (2002) 205.
[43] Borexino Collaboration, G. Alimonti, et al., Nucl. Instrum. Methods A 406 (1998) 411.
[44] E. Resconi, Doctorate thesis, Università degli Studi di Genova, 2001.
[45] Borexino Collaboration, G. Alimonti, et al., Phys. Lett. B 422 (1998) 349.
[46] Borexino Collaboration, G. Alimonti, et al., Astropart. Phys. 8 (1998) 141.
[47] Borexino Collaboration, G. Alimonti, et al., Nucl. Instrum. Methods A 440 (2000) 360.

[48] G. Ranucci, et al., Nucl. Instrum. Methods A 333 (1993) 553.
[49] J.B. Birks, Proc. Phys. Soc. A 64 (1951) 874.
[50] J.M. Los Arcos, F. Ortiz, Comput. Phys. Commun. 103 (1997) 83.
[51] Borexino Collaboration, H.O. Back, et al., Phys. Lett. B 525 (2002) 29.
[52] O.Ju. Smirnov, Instrum. Exp. Tech. 46 (2) (2003), in press.
[53] V.V. Kuzminov, N.Ja. Osetrova, Yad. Fiz. 63 (2000) 365; V.V. Kuzminov, N.Ja. Osetrova, Phys. At. Nucl. 63 (2000) 1292.
[54] J.N. Bahcall, H. Pinsonneault, S. Basu, Astrophys. J. 555 (2001) 990.
[55] J.N. Bahcall, Phys. Rev. C 56 (1997) 3391.
[56] KamLAND Collaboration, K. Eguchi, et al., Phys. Rev. Lett. 90 (2003) 021802.
[57] S.T. Petcov, Yad. Fiz. 25 (1977) 641.
[58] E. Sato, M. Kobayashi, Prog. Theor. Phys. 58 (1977) 1775.
[59] M.A. Beg, W.J. Marciano, M. Ruderman, Phys. Rev. D 17 (1978) 1395.
[60] A. De Rujula, S.L. Glashow, Phys. Rev. Lett. 45 (1980) 942.
[61] P.B. Pal, L. Wolfenstein, Phys. Rev. D 25 (1982) 766.
[62] A.V. Derbin, O.Ju. Smirnov, JETP Lett. 76 (2002) 483.
[63] F. Reines, et al., Phys. Rev. Lett. 32 (1974) 180.
[64] P. Vogel, Phys. Rev. D 30 (1984) 1505.
[65] G. Zacek, et al., Phys. Rev. D 34 (1986) 2621.
[66] L. Oberauer, F. Von Feilitzsch, R.L. Mössbauer, Phys. Lett. B 198 (1987) 113.
[67] A.V. Derbin, et al., JETP Lett. 57 (1993) 768.
[68] D.A. Krakauer, et al., Phys. Rev. D 44 (1991) 44.
[69] G.G. Raffelt, Phys. Rev. D 31 (1985) 3002.
[70] L. Oberauer, et al., Astropart. Phys. 1 (1993) 377.